New Spectral Representation and Dissimilarity Measures Assessment for FTIR-spectra using Unsupervised Classification

Francisco Peñaranda[1], Fernando López-Mir[1], Valery Naranjo[1], Jesús Angulo[2], Lena Kastl[3] and Juergen Schnekenburger[3]

[1] *Instituto Interuniversitario de Investigación en Bioingeniería y Tecnología Orientada al Ser Humano, Universitat Politècnica de Valencia, Valencia, Spain*

[2] *CMM-Centre de Morphologie Mathématique, Mathématiques et Systèmes, MINES Paristech, Fontainebleau, France*

[3] *Biomedical Technology Center, University of Muenster, D-48149, Muenster, Germany*

Keywords: FTIR-spectroscopy, Hyperspectral Imaging, Dissimilarity Measures, Clustering, Cancer.

Abstract: In this work, different combinations of dissimilarity coefficients and clustering algorithms are compared in order to separate FTIR data in different classes. For this purpose, a dataset of eighty five spectra of four types of sample cells acquired with two different protocols are used (fixed and unfixed). Five dissimilarity coefficients were assessed by using three types of unsupervised classifiers (K-means, K-medoids and Agglomerative Hierarchical Clustering). We introduce in particular a new spectral representation by detecting the signals' peaks and their corresponding dynamics and widths. The motivation of this representation is to introduce invariant properties with respect to small spectra shifts or intensity variations. As main results, the dissimilarity measure called *Spectral Information Divergence* obtained the best classification performance for both treatment protocols when is used over the proposed spectral representation.

1 INTRODUCTION

Early diagnosis of cancer is one of the most effective ways for reducing the mortality of this disease (Carter et al., 2013). However, the classification of healthy and unhealthy tissue in some stages of the pathology is a difficult task using current optical imaging or visual inspection. Chemical images have been developed to define not only anatomical structure, but also molecular properties (Petibois and Deleris, 2006). This is the case of Fourier Transform Infra-Red (FTIR) images, which are based on the amount of light that molecules absorb in the range of IR wavelengths or wavenumbers. FTIR images are cubes of hyperspectral signals where one 2D image represents the absorption of the tissue for a specific wavenumber and if a spatial point (x_0, y_0) is fixed, a particular spectrum is obtained (Fig. 1).

FTIR spectroscopy, applied to the diagnosis of cancer, is still a developing research area, dating the pioneer studies from the beginning of this century (Kendall et al., 2009). In this context, the majority of studies only considers the Euclidean distance as a measure of dissimilarity for any kind of classification task. For example, in (Krafft et al., 2008) and (Nallala et al., 2014), unsupervised classification is used for segmentation purposes with this type of measure and K-means algorithm. Another point that has not been questioned in the related literature is the election of the clustering algorithm. The only publication that tries to compares different performances of clustering algorithms (K-means, Fuzzy C-means and Agglomerative Hierarchical Clustering) is (Lasch et al., 2004). Unfortunately, all these studies only analyse the classification performance in a qualitative way.

In this work the ability to arrange different cells spectra by combining five dissimilarity coefficients with three unsupervised classifiers is evaluated by means of objective indices. The raw data and a new spectral representation based on main features of the signal are analysed as inputs of these algorithms.

Section 2 defines the materials, the dissimilarity coefficients and clustering techniques used in this work as well as the proposed new spectral representation. In Section 3, the results of the classification task are shown and they are discussed in Section 4. Finally, Section 5 presents the conclusions of this work.

Peñaranda F., López-Mir F., Naranjo V., Angulo J., Kastl L. and Schnekenburger J..
New Spectral Representation and Dissimilarity Measures Assessment for FTIR-spectra using Unsupervised Classification.
DOI: 10.5220/0005188001720177
In *Proceedings of the International Conference on Bio-inspired Systems and Signal Processing* (BIOSIGNALS-2015), pages 172-177
ISBN: 978-989-758-069-7

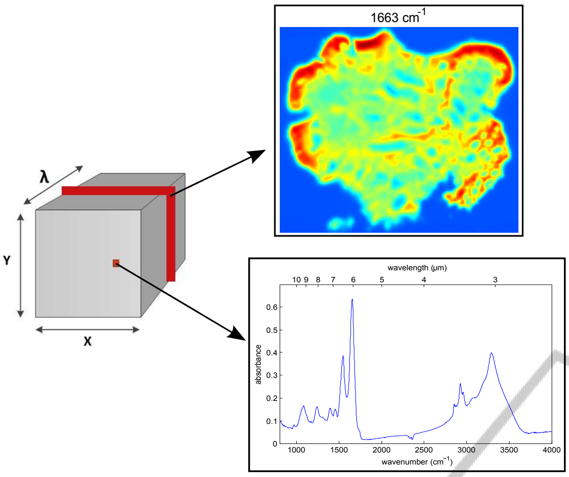

Figure 1: FTIR images. *Left*: Data cube associated to the hyperspectral image. *Right*, *top*: Pseudocolor image representing the spatial absorbance values for a constant wavenumber. *Right*, *bottom*: Absorbance spectrum corresponding to a specific spatial point of the data cube.

2 METHOD

2.1 Spectral Data

Eighty-five spectra of different types of cells were measured using CaF_2 as substrates for the culture and preparation. The cells are divided in four groups: A-375 and SK-MEL-28 cell samples are two skin cancer cell types and HaCaT and NIH-3T3 cell samples represent the two major cellular skins: keratinocytes and fibroblasts. Fifty-eight cell samples were fixed with glutaraldehyde, dehydrated with ethanol and air dried before measurements. Twenty-seven were unfixed in cell media and air dried immediately before measuring. Table 1 summarises this information.

The spectra were measured in transmission mode with an *IFS 66v/S* spectrometer from *Bruker Optics* equipped with a *SiC* global source and a *DLaTGS* detector. The acquisition software subtracted automatically the reference spectrum of the associated CaF_2 window. Each spectrum was acquired between wavenumbers 1000-4000 cm^{-1} with a resolution of 1 cm^{-1}, what results in a vector of 3000 components.

In the pre-processing steps absorbance (A) was calculated from transmittance (T) as $A = -log_{10}(T)$ and a Savitzky-Golay smoothing filter with a window of 31 points and third-order fitted polynomial was applied (Rinnan et al., 2009). Finally, each spectral vector was normalised with its Euclidean norm as $\mathbf{x}_{norm} = \mathbf{x}/||\mathbf{x}||$ (Baker et al., 2008). The normalisation is necessary to minimise possible artefacts during the acquisition process of the IR light (Lasch, 2012).

Table 1: Number of available spectral samples for each kind of cancerous (A-375, SK-MEL-28) and normal (Ha-CaT, NIH-3T3) cells, divided by type of treatment protocol.

Type	**Cancer**		**Normal**		**Total**
	A	**SK**	**HA**	**NIH**	
Fixed	11	22	10	15	**58**
Unfixed	11	8	8	0	**27**

2.2 Dissimilarity Measures

Five dissimilarity coefficients were implemented using Matlab software. A distance matrix ($d_{i,j}$) was obtained, where each value measures the dissimilarity between signals i and j according to the selected coefficient. This distance matrix is symmetric with values equal to zero in the diagonal and positive values out of it. The dissimilarity coefficients assessed were:

- **Euclidean Distance.** It is the most intuitive and fastest measure which is computed by the root of the square differences between the coordinates of a pair of vectors.
- **City Block Distance.** Also known as Manhattan distance, it measures the absolute difference between the coordinates of two spectral vectors.
- **Cosine Distance.** It is computed as 1 minus the cosine between two spectral vectors. Hence, two spectral vectors with a zero angle between them has a cosine distance equals to zero.
- **Correlation Distance.** It is a special case of angular separation standardised by centring the coordinates on its mean and is computed as 1 minus the correlation coefficient.
- **Spectral Information Divergence (*SID*).** It is based on Spectral Information Measure (*SIM*) (Chang, 2003) that considers the inter-band variability as a result of uncertainty incurred by randomness and models the spectral vector as a probability distribution. In the context of information theory, *SID* is the symmetrised version of Kullback-Leibler divergence, which measures the relative entropy provided by each spectral vector.

2.3 Gaussian Model

A new representation of the spectrum is introduced to take into account the most relevant information of its the main peaks. The regional maxima of the signal were found automatically and only the absolute maxima in a neighbourhood of twenty samples were selected to discard noisy maxima. In the peaks obtained after this filter, the dynamic of each peak and its width were computed.

Algorithm 1 summarises the process for obtaining these two features. A reconstruction by dilation was carried out in the spectrum where h was a constant value for each iteration (Soille, 2002). The values of h spanned from 0 to h_{max}, which is equal to the difference between the maximum and the minimum of each spectrum, and $\Delta h = h_{max}/100$. The residue was computed and the *cross-by-zero* around each peak calculated for obtaining two wavenumbers. If these wavenumbers fulfilled some restrictions with the wavenumbers of the maximum neighbours, the h value was considered as the dynamic and the width was extracted directly as the difference of the two wavenumbers. Fig. 2a shows, in a specific signal, the properties of each peak obtained with this process.

Algorithm 1: Extraction of peaks' dynamic and width.

```
x = spectrum with relevant maxima detected at wavenumbers $A_1, \ldots, A_n$
For each peak ($i = 1 : n$)
  For $h = 0 : (h_{max}/100) : h_{max}$
    Y = reconstruction (x, x-h)
    R = x - Y
    Follow the two cross-by-zero in R around the peak to obtain two wavenumbers ($w_1, w_2$)
    If ($w_1 > A_{i-1}$ AND $w_2 < A_{i+1}$)
      $Dynamic_i = h$
      $Width_i = w_2 - w_1$
      Go to next peak
    End if
  End h
End peak
```

A Dirac delta function with an intensity equals to the corresponding dynamic was positioned in each peak's wavenumber. Each Dirac delta was convolved with a Gaussian function: $e^{-\frac{w^2}{2\sigma^2}}$, where w is the wavenumber variable and $\sigma = width_{peak}$. Finally, the resulting convolutions were added to form an equivalent spectral representation that contains relevant information of the original spectrum, Fig. 2b.

The aim of this model is to represent the most important information within the signal in a more robust and simpler way. Finding only the features of the principal peaks the noise due to different sources as scattering, which causes additive and multiplicative intensity artefacts, is reduced. By convolving the Dirac deltas with an adaptive Gaussian function, the model tries to be more robust against small changes or shifts in the position of the peaks, which can also be produced by scattering effects and even imperfections in the spectroscopic light sensor.

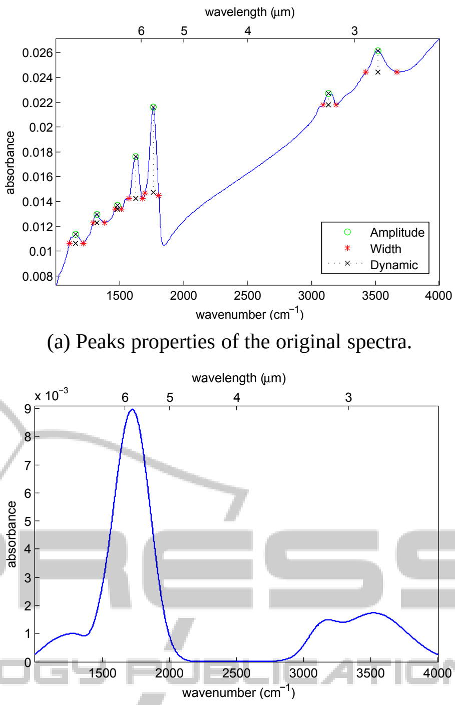

(a) Peaks properties of the original spectra.

(b) Gaussian model representation.

Figure 2: Proposed spectral Gaussian model.

2.4 Unsupervised Classification

There is a wide variety of clustering algorithms with different characteristics due to their distinct ways to group a dataset and the measure of similarity or dissimilarity is data dependent (Bandyopadhyay and Saha, 2013). Hence, it is important to compare the performance of different combinations of classification methods and distance coefficients.

Three types of clustering algorithms were used to assess how suitable the studied dissimilarity measures are for correctly discriminating the spectral samples. In these techniques, the number of clusters k must be specified ($k = 4$ in fixed and $k = 3$ in unfixed cells).

- **K-means (*KM*).** It is the most popular clustering algorithm used in many fields of interest. It is a partitioning algorithm that divides data into k subsets represented by their *centroids*, which are calculated by the mean or weighted average of the cluster members. The iterative partitioning minimises an objective function based on the Euclidean norm that represents the total intra-cluster variance. There are a lot of variations of this algorithm in the literature (Berkhin, 2006; Jain, 2010). In this algorithm only the former four distances described in Sec. 2.2 can be implemented due to the definition of the objective function.

- **K-medoids (*Kmd*).** It is another popular partitioning clustering algorithm. This is an extension of *KM* where the concept of *medoid* (a representative data point from the dataset) is used instead of the *centroid*. *Kmd* minimizes a sum of pairwise dissimilarities instead of a sum of squared Euclidean distances (Bandyopadhyay and Saha, 2013), so, the five studied distances can be implemented. *Kmd* is more robust to noise and outliers than *KM* because the computation of *medoids* is dictated by the location of a predominant fraction of points inside a cluster (Berkhin, 2006).
- **Agglomerative Hierarchical Clustering (*AHC*).** It builds a hierarchy of clusters starting with one-point (singleton) clusters and recursively merges two or more of the most similar clusters as one moves up the hierarchy. The linkage clustering technique is a non-iterative process based on a local connectivity criterion. The four methods of linkage used in this paper differ in the definition of the distance between clusters:
  - *Single linkage* utilizes the smallest distance between points in the two clusters.
  - *Complete linkage* makes use of the largest distance between points in the two clusters.
  - *Average linkage* uses the average distance between all pairs of points in any two clusters.
  - *Weighted average linkage* uses a recursive definition for the distance between two clusters.

2.4.1 Performance Measures

Three indices were used to assess the performance of the clustering algorithms with the dissimilarity coefficients. The first index, the *Overall Accuracy (OA)*, measures the accuracy to group the spectra in their correct type of cell and is defined as:

$$OA(\%) = \frac{\sum_{i=1}^{k} c_{ii}}{\sum_{i=1}^{k}\sum_{j=1}^{k} c_{ij}} \cdot 100, \tag{1}$$

where c_{ij} is the number of spectra classified as class j and referenced as class i. The second group of indices evaluates the results from a diagnostic point of view. These are the well known *Sensitivity (Sn)* and *Specificity (Sp)*, defined as:

$$Sn(\%) = \frac{TP}{TP+FN} \cdot 100,\ Sp(\%) = \frac{TN}{TN+FP} \cdot 100 \tag{2}$$

where TP are the *True Positives* (cancer cells correctly classified), FN are the *False Negatives* (cancer cells incorrectly classified), TN are the *True Negatives* (normal cells correctly classified) and FP are the *False Positives* (normal cells incorrectly classified).

3 RESULTS

The different combinations of dissimilarity measures and clustering algorithms using the pre-processed raw spectra and the proposed Gaussian model are evaluated in Table 2. Cell samples were studied separately depending on their chemical treatment protocol because it has a crucial influence in the properties of spectra. Results for fixed cells are presented in the top part of Table 2 and unfixed cells in the bottom part.

Although the four described linkage methods for *AHC* were implemented, only the results for *single linkage* are shown because they obtained the highest *OA*. *Sn* and *Sp* are shown because they give important information for diagnosis; nevertheless, *OA* is the chosen index to select the best combinations because it condenses the efficiency of the classifications in the actual type of cells, not only considering if they are normal or pathological (Table 1). For each treatment protocol, the highest *OA* is highlighted.

In fixed cells, if the pre-processed raw spectra is used, the best similarity measure is the city block distance with *KM* as well as *Kmd*, although the Euclidean distance also has a close efficiency with *Kmd* and *AHC*. On the other hand, the Gaussian model has an equivalent *OA* if *Kmd* is used with SID, although the cosine distance with *KM* and *Kmd* has a slightly low performance. The *Sn* values for the highest *OA* are equivalent in the two spectral representations but the Gaussian model has a higher *Sp*.

In unfixed cells, the results of the Gaussian model looks impressive since the 100% of *OA* is obtained for any dissimilarity measure using *Kmd* and using cosine and correlation distance with *KM*. In the case of the pre-processed raw spectra, the results are also very satisfactory for *Kmd* with Euclidean and city block distance. The *Sn* and *Sp* are also maximum for the best *OA* obtained with the Gaussian model. However, the performance results can be very low for some combinations, mainly the *Sp* index.

4 DISCUSSION

The performance values seems to be really promising for some combinations, but the results must be taken with caution mainly due to the small number of available samples, especially in unfixed cells.

Another related problem is the different number of cell types for each kind of treatment protocol (Table 1). In fixed cells, the number of SK-MEL-28 (22 samples) is higher than the rest of cell types, what might have affected the value of *OA* because the classification of this type of cells has a higher weight in its cal-

Table 2: Results of performance of the different combinations of dissimilarity measures and clustering algorithms for the two types of treatment protocols (Above: Fixed, Below: Unfixed), using the pre-processed raw spectra and the proposed Gaussian model. (*OA: Overall Accuracy*, *Sn: Sensitivity*, *Sp: Specificity*).

Fixed							
			Euclidean	City Block	Cosine	Correlation	SID
K-means	Raw Spectra	OA	79.3	**93.1**	79.3	81	
		Sn	100	93.9	100	100	-
		Sp	100	100	100	100	
	Gaussian	OA	79.3	89.7	91.4	82.8	
		Sn	100	100	93.9	93.9	-
		Sp	100	100	92	72	
K-medoids	Raw Spectra	OA	91.4	**93.1**	81	81	79.3
		Sn	93.9	93.9	100	100	100
		Sp	100	100	100	100	100
	Gaussian	OA	81	89.7	91.4	82.8	**93.1**
		Sn	100	100	93.9	93.9	93.9
		Sp	100	100	92	72	96
Hierarchical	Raw Spectra	OA	91.4	82.8	81	69	72.4
		Sn	84.8	100	100	90.9	100
		Sp	100	100	100	40	80
	Gaussian	OA	74.1	72.4	65.5	50	65.5
		Sn	84.8	84.8	84.8	84.8	84.8
		Sp	100	100	44	4	48

Unfixed							
			Euclidean	City Block	Cosine	Correlation	SID
K-means	Raw Spectra	OA	59.3	96.3	59.3	59.3	
		Sn	84.2	94.7	57.9	84.2	-
		Sp	0	100	100	0	
	Gaussian	OA	59.3	59.3	**100**	**100**	
		Sn	84.2	57.9	100	100	-
		Sp	0	100	100	100	
K-medoids	Raw Spectra	OA	96.3	96.3	59.3	59.3	59.3
		Sn	94.7	94.7	84.2	84.2	84.2
		Sp	100	100	0	0	0
	Gaussian	OA	**100**	**100**	**100**	**100**	**100**
		Sn	100	100	100	100	100
		Sp	100	100	100	100	100
Hierarchical	Raw Spectra	OA	59.3	59.3	59.3	59.3	59.3
		Sn	57.9	57.9	57.9	84.2	57.9
		Sp	100	100	100	0	100
	Gaussian	OA	59.3	55.6	74.1	66.7	77.8
		Sn	57.9	78.9	100	57.9	68.4
		Sp	100	0	12.5	100	100

culation. In unfixed cells, the number of samples of different cell types is quite balanced, but the number of cancer (19 samples) and normal cells (8 samples) is very different, so in this case the unbiased indices are *Sn* and *Sp*. This fact is more important for *Sp* index because if the separation of the 8 normal samples fails its value is really low or even zero.

In spite of these problems, the obtained results are valuable because they demonstrate that the election of the dissimilarity measure along with the clustering algorithm is important for the classification performance. This fact should be taken into account in another clustering applications of FTIR data, where only the Euclidean distance is commonly utilised (Sec. 1).

5 CONCLUSIONS

A methodology for studying the ability of five dissimilarity coefficients to correctly separate hyperspectral data was carried out. For this purpose three different clustering algorithms were used to gather eighty five spectra in their corresponding types of cell. These spectra belonged to two different groups due to the two different protocols used in the acquisition step.

As a novelty, a new spectral representation model has been described. This method extracts the main features enclosed in the principal peaks of the spectrum and translates them into a signal that can be more robust against scattering and sensor's artefacts.

As main conclusion of this study, not only the optimal dissimilarity measure is data dependent, but also the optimal clustering algorithm. It is necessary to extend this study to new spectral data to be able to generalise the results. Nevertheless, the Spectral Information Divergence has obtained the best overall results in the classification task when is applied over the proposed Gaussian model in both treatment protocols.

The future steps will be the comparison of other dissimilarity coefficients and more complex clustering algorithms in new FTIR datasets containing more samples. As inputs of the algorithms, new ways to represent the main information of spectra (PCA and Sparse Representation) will be studied and compared with the proposed Gaussian model, which will be improved to contain other significant signal properties.

ACKNOWLEDGEMENTS

This research has been supported by the European Commission through the Framework Seven project MINERVA (317803; www.minerva-project.eu).

REFERENCES

Baker, M., Gazi, E., Brown, M., Shanks, J., Gardner, P., and Clarke, N. (2008). FTIR-based spectroscopic analysis in the identification of clinically aggressive prostate cancer. *Br J Cancer*, 99(11):1859–66.

Bandyopadhyay, S. and Saha, S. (2013). *Unsupervised Classification: Similarity Measures, Classical and Metaheuristic Approaches, and Applications*. Springer.

Berkhin, P. (2006). A survey of clustering data mining techniques. In *Grouping multidimensional data*, pages 25–71. Springer.

Carter, H. B., Albertsen, P., Barry, M., Etzioni, R., Freedland, S., Greene, K., Holmberg, L., Kantoff, P., Konety, B., Murad, M., Penson, D., and Zietman, A. (2013). Early detection of prostate cancer: AUA guideline. *The Journal of Urology*, 190(2):419 – 26.

Chang, C.-I. (2003). *Hyperspectral imaging: techniques for spectral detection and classification*, volume 1. Springer.

Jain, A. K. (2010). Data clustering: 50 years beyond k-means. *Pattern Recognition Letters*, 31(8):651–666.

Kendall, C., Isabelle, M., Bazant-Hegemark, F., Hutchings, J., Orr, L., Babrah, J., Baker, R., and Stone, N. (2009). Vibrational spectroscopy: a clinical tool for cancer diagnostics. *Analyst*, 134(6):1029–1045.

Krafft, C., Codrich, D., Pelizzo, G., and Sergo, V. (2008). Raman and ftir microscopic imaging of colon tissue: a comparative study. *Journal of biophotonics*, 1(2):154–169.

Lasch, P. (2012). Spectral pre-processing for biomedical vibrational spectroscopy and microspectroscopic imaging. *Chemometrics and Intelligent Laboratory Systems*, 117:100–114.

Lasch, P., Haensch, W., Naumann, D., and Diem, M. (2004). Imaging of colorectal adenocarcinoma using ft-ir microspectroscopy and cluster analysis. *Biochimica et Biophysica Acta (BBA)-Molecular Basis of Disease*, 1688(2):176–186.

Nallala, J., Piot, O., Diebold, M.-D., Gobinet, C., Bouché, O., Manfait, M., and Sockalingum, G. D. (2014). Infrared and raman imaging for characterizing complex biological materials: A comparative morpho-spectroscopic study of colon tissue. *Applied spectroscopy*, 68(1):57–68.

Petibois, C. and Deleris, G. (2006). Chemical mapping of tumor progression by FT-IR imaging: towards molecular histopathology. *Trends in Biotechnology*, 24(10):455 – 62.

Rinnan, A., Berg, F. v. d., and Engelsen, S. B. (2009). Review of the most common pre-processing techniques for near-infrared spectra. *TrAC Trends in Analytical Chemistry*, 28(10):1201–1222.

Soille, P. (2002). *Morphological Image Analysis*, volume Second edition. Springer.